Electronic Supplementary Information

Dynamic Bond Interaction Fine-Tunes the Properties of Multiple Resonance Emitters towards Highly Efficient Narrowband Green OLEDs

Yang Zou, Mingxin Yu, Jingsheng Miao, Taian Huang, Shuokun Liao, Xiaosong Cao, Chuluo Yang*

Shenzhen Key Laboratory of New Information Display and Storage Materials, College of Materials Science and Engineering, Shenzhen University, Shenzhen 518060, PR China

Jingsheng Miao email: jingshengmiao@szu.edu.cn

General information

Unless otherwise indicated, all starting materials were obtained from commercial suppliers and were used without further purification. All the reaction solvents were purified by solvent purification system prior to use.

The ^{1}H and ^{13}C nuclear magnetic resonance (NMR) spectra were recorded in deuterated chloroform ($CDCl_3$) solution on Bruker NMR spectrometer with tetramethylsilane (TMS, δ 0.00) as the internal standard. High-resolution electrospray (ESI) mass spectra were performed on SCIEX TripleTOF6600 nanoLCMS. Thermogravimetric analysis (TGA) was undertaken using a PerkinElmer Instruments (Pyris1 TGA) at a heating rate of 10 °C per min from 30 to 800 °C under a nitrogen environment. UV-vis absorption spectra were recorded on a Shimadzu UV-2700 recording spectrophotometer. Photoluminescence (PL) spectra were recorded on a Hitachi F-4600 fluorescence spectrophotometer. The lifetimes of fluorescence and delayed fluorescence were performed on PicoQuant Fluotime300. Absolute PLQYs were obtained using a Quantaurus-QY measurement system (C9920-02, Hamamatsu

Photonics). Cyclic voltammetry (CV) was carried out in nitrogen-purged dichloromethane (oxidation scan) at room temperature with a CHI voltammetric analyzer. Tetrabutylammonium hexafluorophosphate ($TBAPF_6$) (0.1 M) was used as the supporting electrolyte. The conventional three-electrode configuration consists of a platinum working electrode, a platinum wire auxiliary electrode, and an Ag wire pseudo reference electrode with ferrocenium/ferrocene (Fc^+/Fc) as the internal standard.

Quantum Chemical Calculations: All of the simulation calculations were carried out with Gaussian 09 program package. The ground state geometries were optimized *via* density functional theory (DFT) calculations in vacuum using the B3LYP-D3(BJ) hybrid functional and the 6-31G(d,p) basis set. The density functional dispersion correction was conducted by Grimme's D3 version with Becke-Johnson damping function. Excited state analysis by time-dependent DFT (TD-DFT) were performed at the B3LYP-D3(BJ)/6-31G(d,p) level on the basis of optimized ground-state geometries.

Analysis of Rate Constants: The rate constants of radiative decay ($k_{r,S}$) and nonradiative decay ($k_{nr,S}$) from S_1 to S_0 states, the rate constants of intersystem crossing (k_{ISC}) and reverse intersystem crossing (k_{RISC}) were calculated from the following six equations:

$$k_p = 1/\tau_p \quad \text{Eq.(1)}$$

$$k_d = 1/\tau_d \quad \text{Eq.(2)}$$

$$k_{r,S} = \Phi_p k_p + \Phi_d k_d \approx \Phi_p k_p \quad \text{Eq.(3)}$$

$$k_{nr,S} = \frac{1 - \Phi_{PL}}{\Phi_{PL}} k_{r,S} \quad \text{Eq.(4)}$$

$$k_{ISC} = k_p - k_{r,S} - k_{nr,S} \quad \text{Eq.(5)}$$

$$k_{RISC} = (k_p k_d \Phi_d)/(k_{ISC} \Phi_p) \quad \text{Eq.(6)}$$

Device Fabrication and Characterization: The ITO coated glass substrates with a sheet resistance of 15 Ω square^{-1} were consecutively ultrasonicated with acetone/ethanol and dried with nitrogen gas flow, followed by 20 min ultraviolet light-ozone (UVO) treatment in a UV-ozone surface processor (PL16 series, Sen Lights Corporation). Then the sample was transferred to the deposition system. Both 8-hydroxyquinolinolato-lithium (Liq) as electron injection layer and aluminum (Al) as cathode layer were deposited by thermal evaporation at 5×10^{-5} Pa. Additionally, the organic layers were deposited at the rates of 0.2-3 Å/s. After the organic film deposition, Liq and Al layer were deposited with rates of 0.1 and 3 Å/s, respectively. The emitting area of the device is about 0.09 cm^2. The current density-voltage-luminance (*J-V-L*), L-EQE curves and electroluminescence spectra were measured using a Keithley 2400 source meter and an absolute EQE measurement system (C9920-12, Hamamatsu Photonics, Japan).

OLED optical simulation: The optical simulation tool is based on the equivalence between molecular emission through electronic dipole transitions and radiation from classical electrical dipole antenna. With plane-wave expansion of a dipole field (with each plane-wave mode being characterized by an in-plane wave vector k_t), electromagnetic fields generated by a radiation dipole embedded in a layered structure was calculated, from which the distribution of the radiation power into different plane-wave modes and the far-field radiation can be obtained. Emission characteristics of an OLED were calculated by assuming that the emitting layer contains an ensemble of mutually incoherent dipole radiators with distributions in orientations, locations, and frequencies. The overall emission characteristics were calculated by locating emitting dipoles in the emitting layer and by considering the orientational distribution using the horizontal dipole ratio (Θ//) measured and the full spectral distribution using the PL spectra of emitting layers of radiating dipoles. In addition, the refractive indexes (*n*)

and extinction coefficient (k) of each material in our device structure were used for calculating the theoretical EQE_{max} (Figure S10).

Synthesis of Materials:

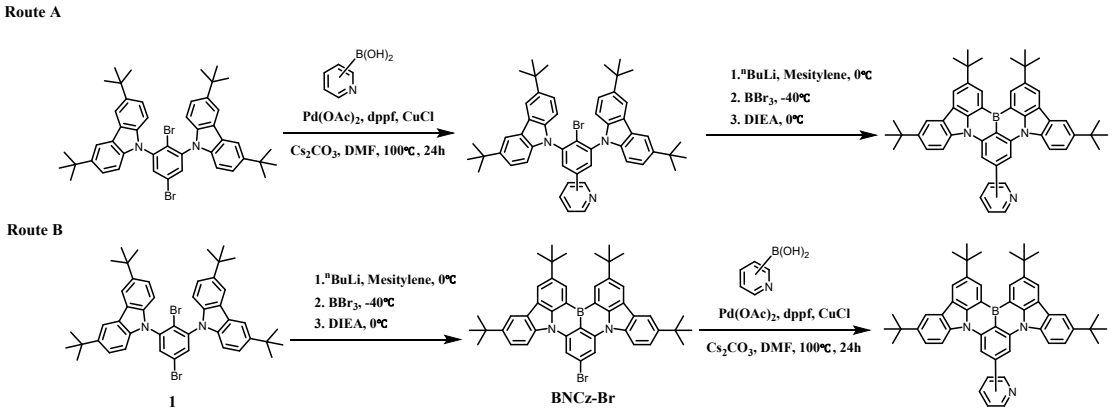

Scheme S1. Synthetic route of **2PyBN**, **2PyBN** and **2PyBN**.

Synthesis of BNCz-Br: To a Schlenk tube was added compound **1** (11.85 g, 15 mmol) and dry mesitylene (80 mL). The mixture was kept in ice-water bath and *n*-BuLi (6.6 mL in hexane, 2.5 M, 16.5 mmol) was added dropwise under argon atmosphere. The reaction mixture was allowed to RT and hexane was removed by vacuum pump. Then under ice-water bath, BBr_3 (2.85 mL, 30 mmol) was injected at once. The reaction mixture was stirred for 15 minutes, allowed to RT and further stirred for another 30 minutes. After adding DIPEA (4.8 mL, 30 mmol), the tube was sealed and the reaction was heated to 180 ℃ and stirred for 12 h. After cooling to RT, the reaction was poured into water, extracted with dichloromethane. After removing all the organic solvents by rotavapor, the crude product was washed thoroughly with DCM:PE (1:10, *v/v*). The crude product was further purified by recrystallization from DCM and hexane to afford **BNCz-Br** as a yellow powder with the yield of 74%. ^{1}H NMR (500 MHz, $CDCl_3$) δ 9.00 (d, J = 1.7 Hz, 2H), 8.79 (s, 3H), 8.42 – 8.37 (m, 4H), 8.20 (d, J = 2.0 Hz, 2H), 7.86 (d, J = 7.8 Hz, 1H), 7.78 (t, J = 7.7 Hz, 1H), 7.66 (dd, J = 8.7, 2.1 Hz, 2H), 7.30 (dd, J = 7.4, 4.9 Hz, 1H), 1.67 (s, 18H), 1.57 (s, 18H). ^{13}C NMR (151 MHz, $CDCl_3$) δ 157.02, 149.95, 145.11, 144.52, 144.46, 143.27, 141.81, 138.41, 136.83, 129.69, 127.09, 124.56, 123.71, 122.86, 121.76, 121.04, 120.67, 117.22, 114.54, 106.46, 35.27, 34.93, 32.34, 32.02. HRMS: (ESI) m/z calcd for $C_{20}H_{16}Cl_2N_2$ [M+H]+: 718.4327;

found: 718.4338.

General procedure for the Suzuki-Miyaura coupling of BNCz-Br with pyridine boronic acid: To a round-bottom flask was added **BNCz-Br** (0.72 g, 1 mmol), pyridine boronic acid (0.25 g, 2 mmol), Pd(dppf)Cl_2 (11 mg, 0.05 mmol), CuCl (0.15 g, 1.5 mmol), Cs_2CO_3 (0.65 g, 2 mmol) and 10 mL dry DMF. The mixture was stirred at 100℃ under argon for 16h. After cooling to room temperature, the reaction mixture was filtered to remove inorganic compounds. After removing DMF by rotavapor, the crude product was further purified by column chromatography on silica gel (eluent: petroleum ether/dichloromethane = 3:1, *v/v*) to afford corresponding compound.

2PyBN: Yellow powder, yield 82%. ^{1}H NMR (500 MHz, $CDCl_3$) δ 9.00 (d, *J* = 1.7 Hz, 2H), 8.79 (s, 3H), 8.42 – 8.37 (m, 4H), 8.20 (d, *J* = 2.0 Hz, 2H), 7.86 (d, *J* = 7.8 Hz, 1H), 7.78 (t, *J* = 7.7 Hz, 1H), 7.66 (dd, *J* = 8.7, 2.1 Hz, 2H), 7.30 (dd, *J* = 7.4, 4.9 Hz, 1H), 1.67 (s, 18H), 1.57 (s, 18H). ^{13}C NMR (126 MHz, $CDCl_3$) δ 157.02, 149.95, 145.11, 144.52, 144.46, 143.27, 141.81, 138.41, 136.83, 129.69, 127.09, 124.56, 123.71, 122.86, 121.76, 121.04, 120.67, 117.22, 114.54, 106.46, 35.27, 34.93, 32.34, 32.02. HRMS: (ESI) m/z calcd for $C_{20}H_{16}Cl_2N_2$ [M+H]+: 718.4327; found: 718.4338.

3PyBN: Yellow powder, yield 79%. ^{1}H NMR (500 MHz, $CDCl_3$) δ 9.06 (d, *J* = 3.8 Hz, 1H), 8.93 (d, *J* = 4.5 Hz, 2H), 8.73 (d, *J* = 4.9 Hz, 1H), 8.37 (dd, *J* = 3.4, 1.7 Hz, 2H), 8.25 – 8.19 (m, 6H), 7.99 (td, *J* = 6.8, 3.8 Hz, 1H), 7.64 – 7.58 (m, 2H), 7.46 (dd, *J* = 6.2, 2.6 Hz, 1H), 1.64 (d, *J* = 1.0 Hz, 18H), 1.55 (s, 18H). ^{13}C NMR (126 MHz, $CDCl_3$) δ 149.20 , 148.73 , 145.47 , 144.69 , 141.70 , 138.23 , 135.03 , 129.69 , 127.24 , 124.55 , 123.88 , 123.67 , 120.84 , 117.45 , 114.32 , 106.48 , 35.27 , 34.94 , 32.29 , 31.98. HRMS: (ESI) m/z calcd for $C_{20}H_{16}Cl_2N_2$ [M+H]+: 718.4327; found: 718.4334.

4PyBN: Yellow powder, yield 72%. ^{1}H NMR (500 MHz, $CDCl_3$) δ 9.05 (d, *J* = 1.9 Hz, 2H), 8.81 (d, *J* = 5.0 Hz, 2H), 8.47 – 8.40 (m, 4H), 8.33 (d, *J* = 8.7 Hz, 2H), 8.25 (d, *J* = 2.1 Hz, 2H), 7.77 (d, *J* = 5.6 Hz, 2H), 7.68 (dd, *J* = 8.7, 2.1 Hz, 2H), 1.66 (s, 18H), 1.54 (s, 18H). ^{13}C NMR (126 MHz, $CDCl_3$) δ 150.16 , 145.75 , 145.07 , 144.91 , 141.80 , 138.27 , 129.86 , 127.34 , 124.70 , 123.79 , 122.53 , 120.90 , 117.59 , 114.16

, 106.63 , 35.33 , 34.98 , 32.31 , 31.97. HRMS: (ESI) m/z calcd for $C_{20}H_{16}Cl_2N_2$ [M+H]+: 718.4327; found: 718.4321.

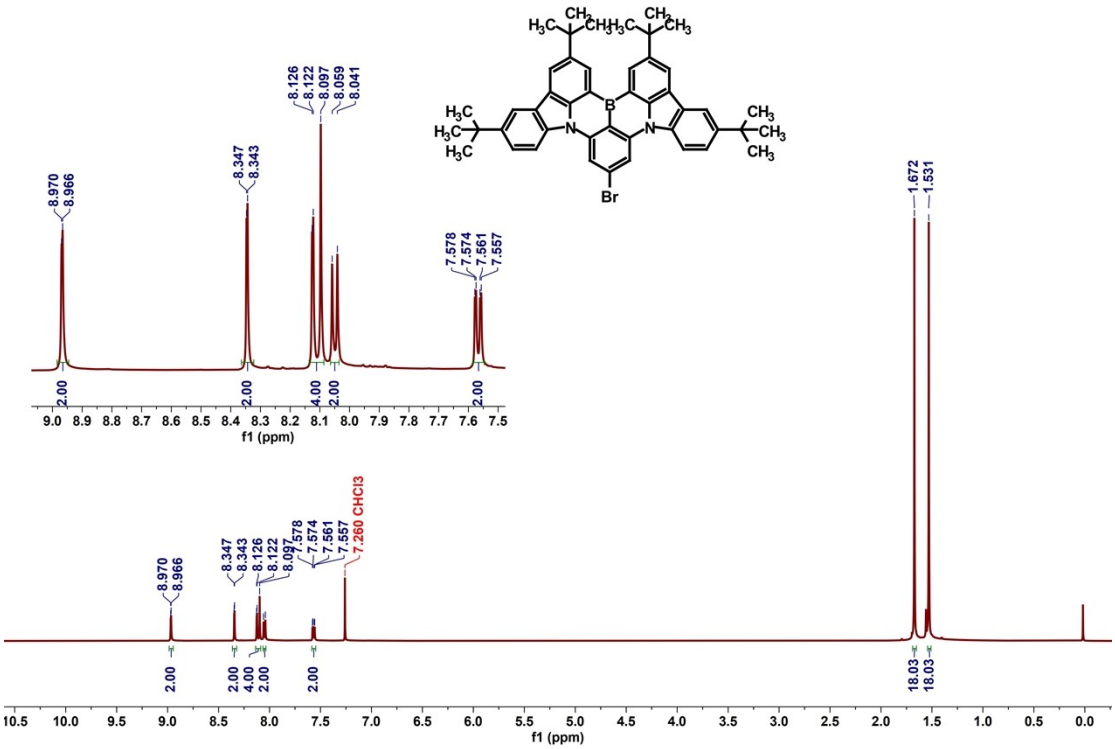

Fig. S1 ^{1}H NMR spectrum of **BNCz-Br**.

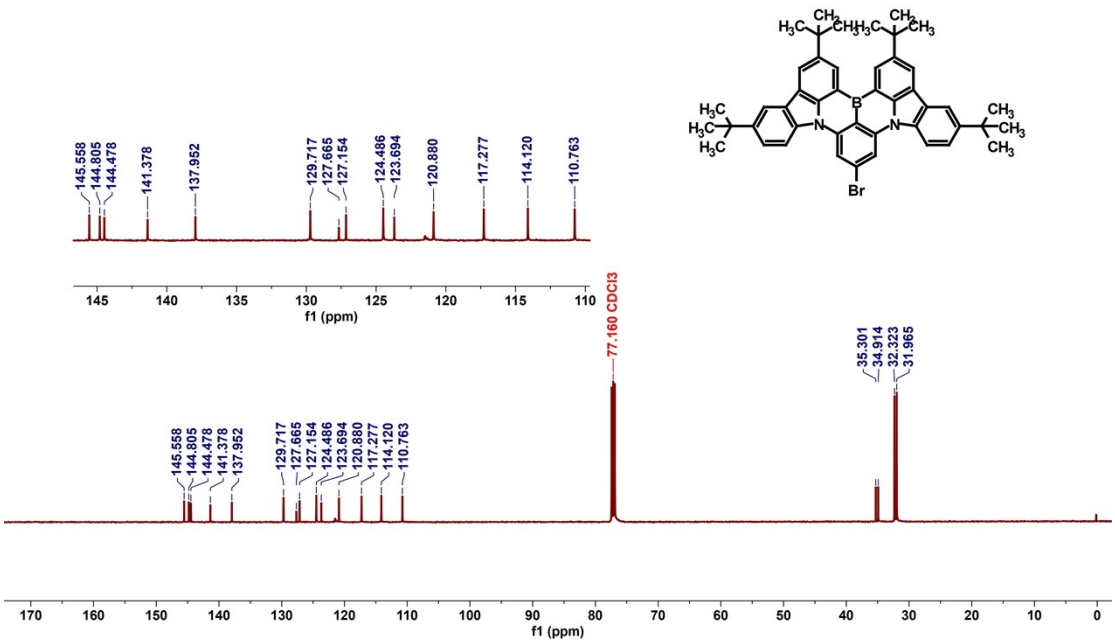

Fig. S2 ^{13}C NMR spectrum of **BNCz-Br**

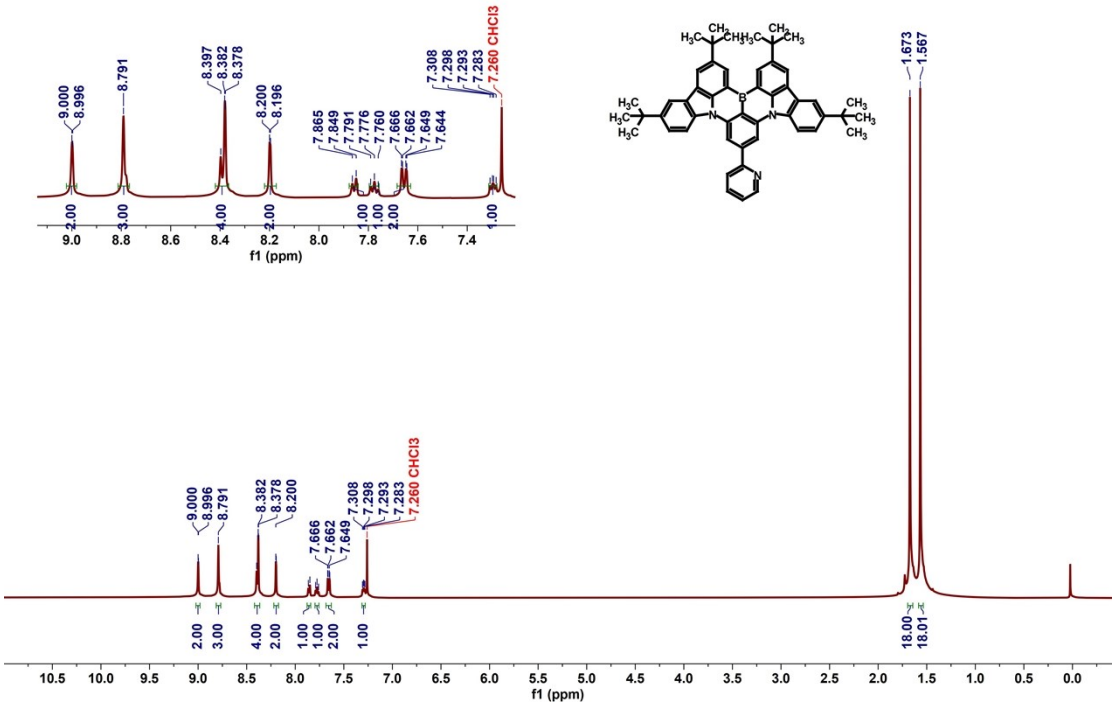

Fig. S3 ^{1}H NMR spectrum of **2PyBN**

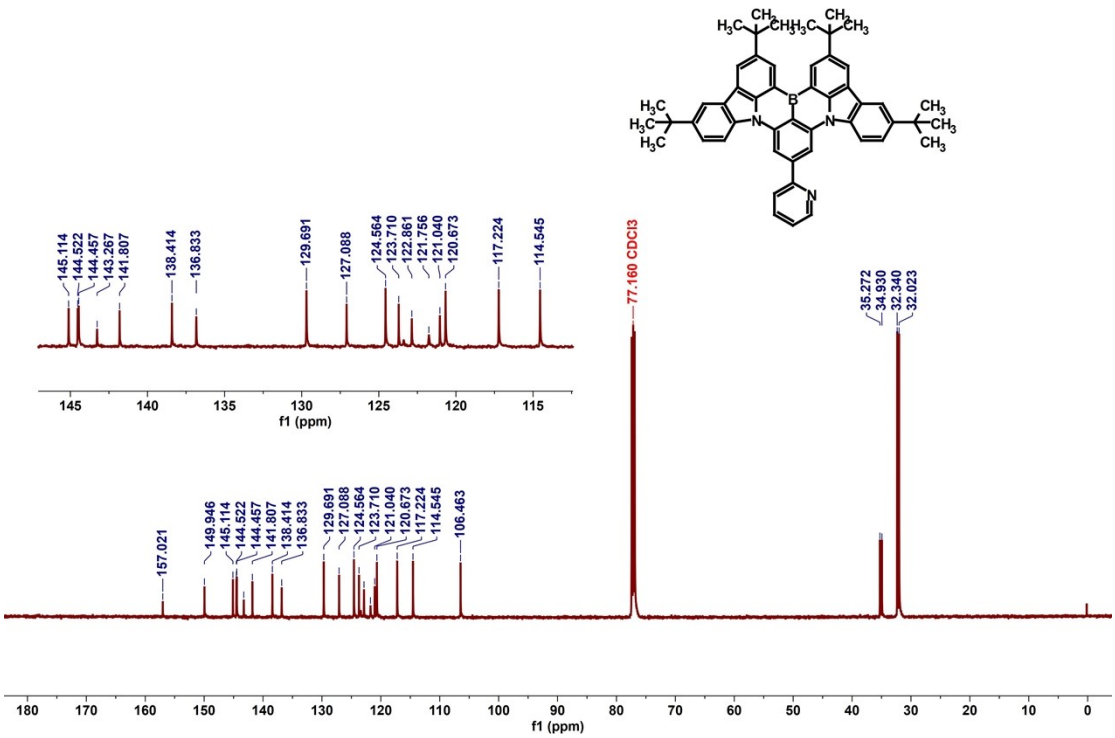

Fig. S4 ^{13}C NMR spectrum of **2PyBN.**

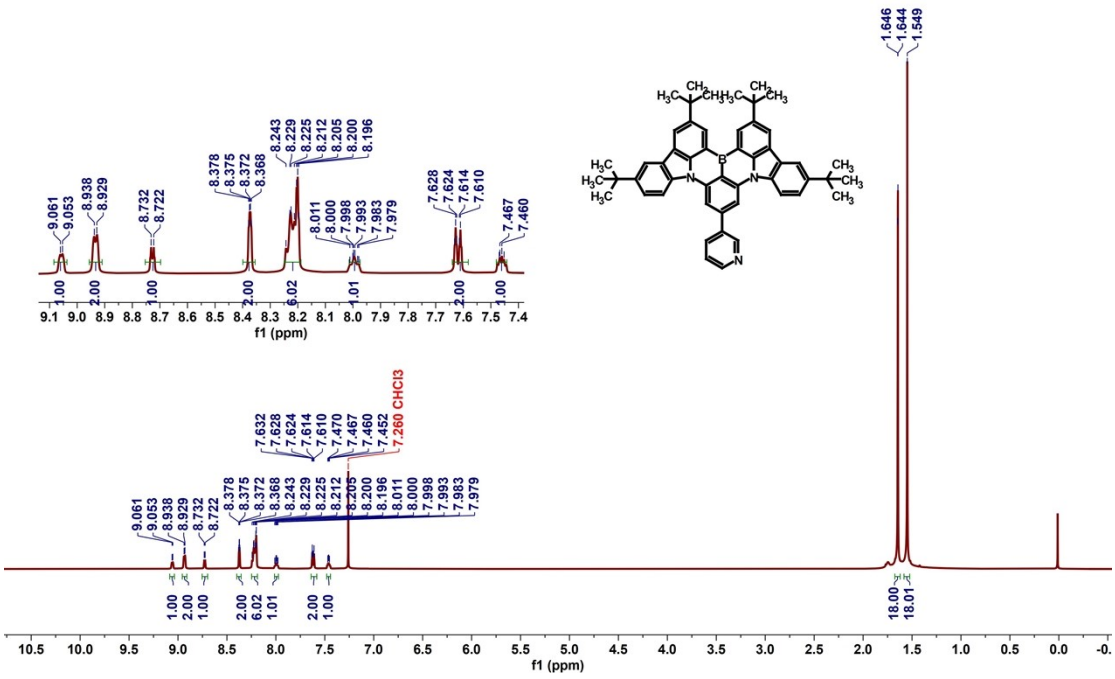

Fig. S5 ^{1}H NMR spectrum of **3PyBN.**

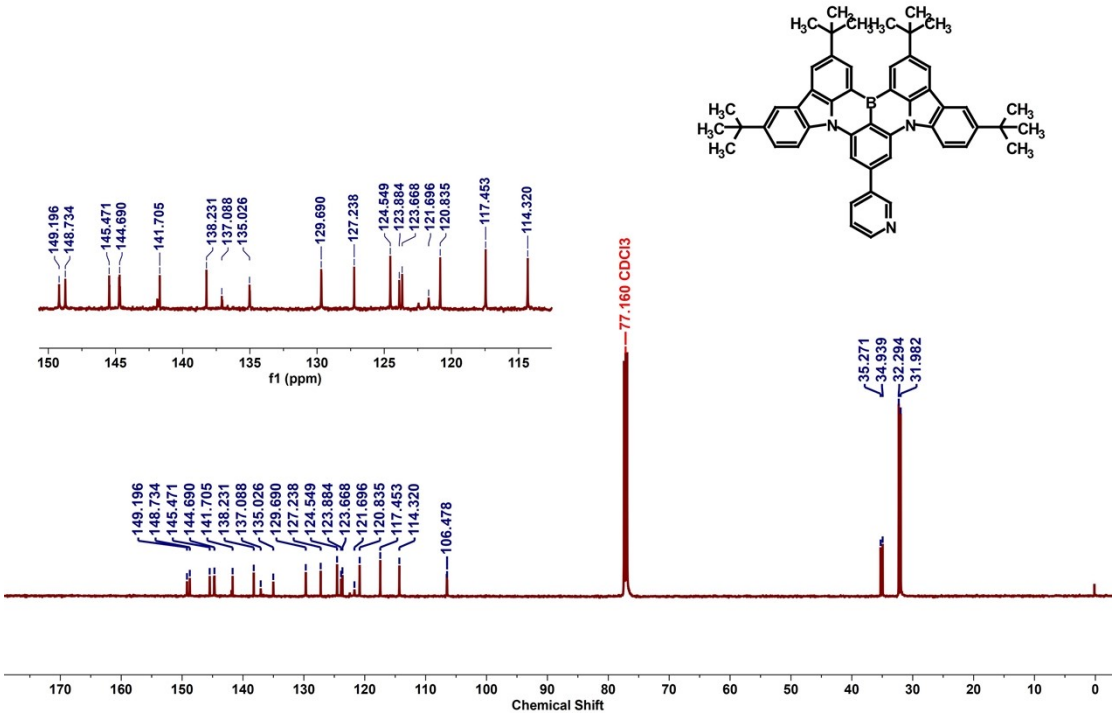

Fig. S6 ^{13}C NMR spectrum of **3PyBN**.

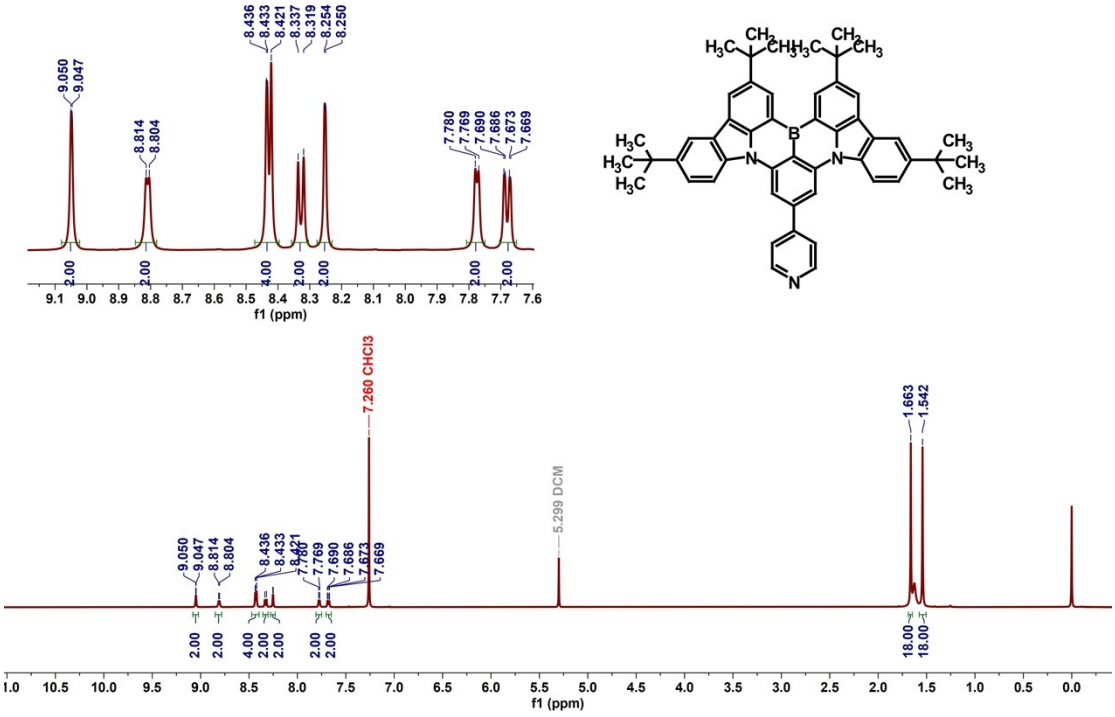

Fig. S7 ^{1}H NMR spectrum of **4PyBN**.

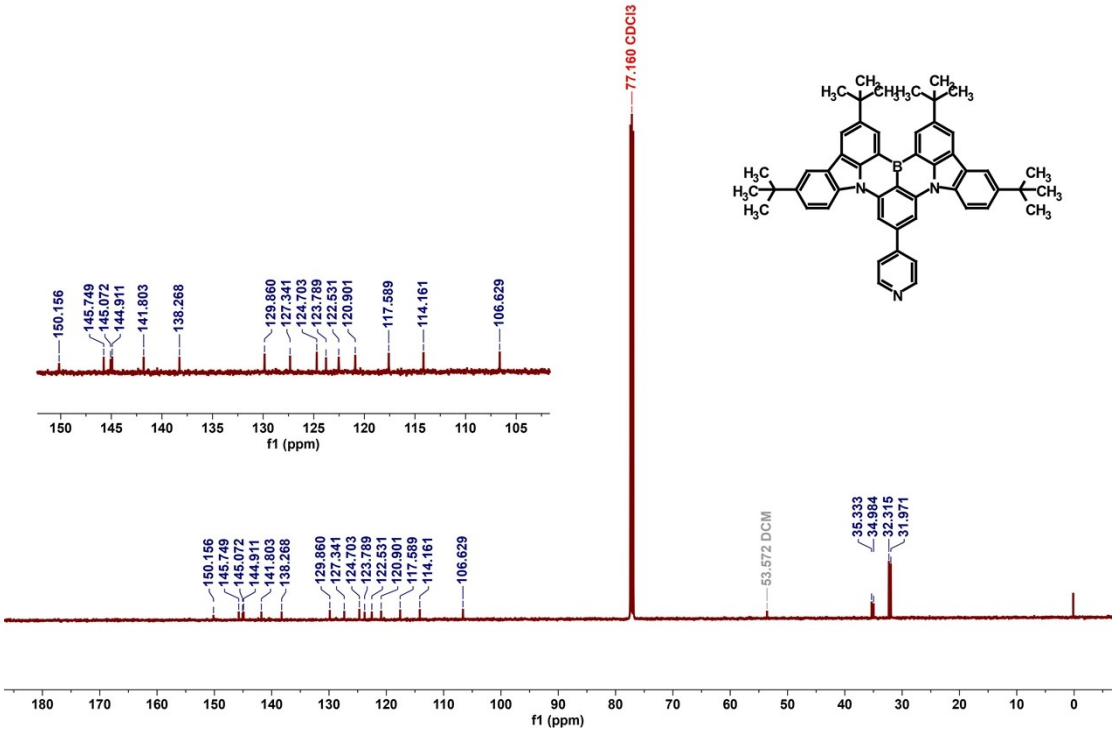

Fig. S8 ^{13}C NMR spectrum of **4PyBN**.

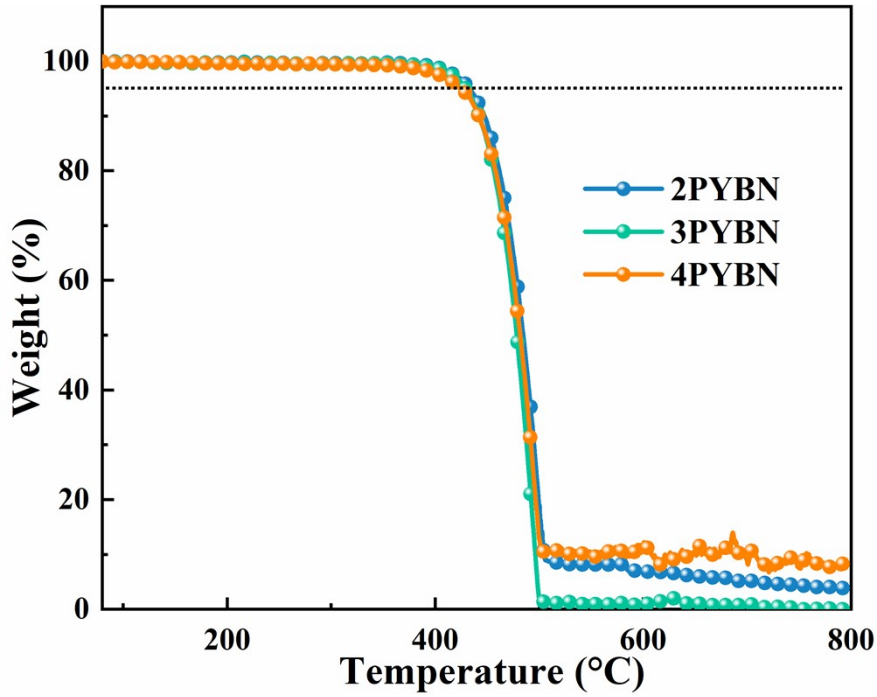

Fig. S9 TGA curves of emitters.

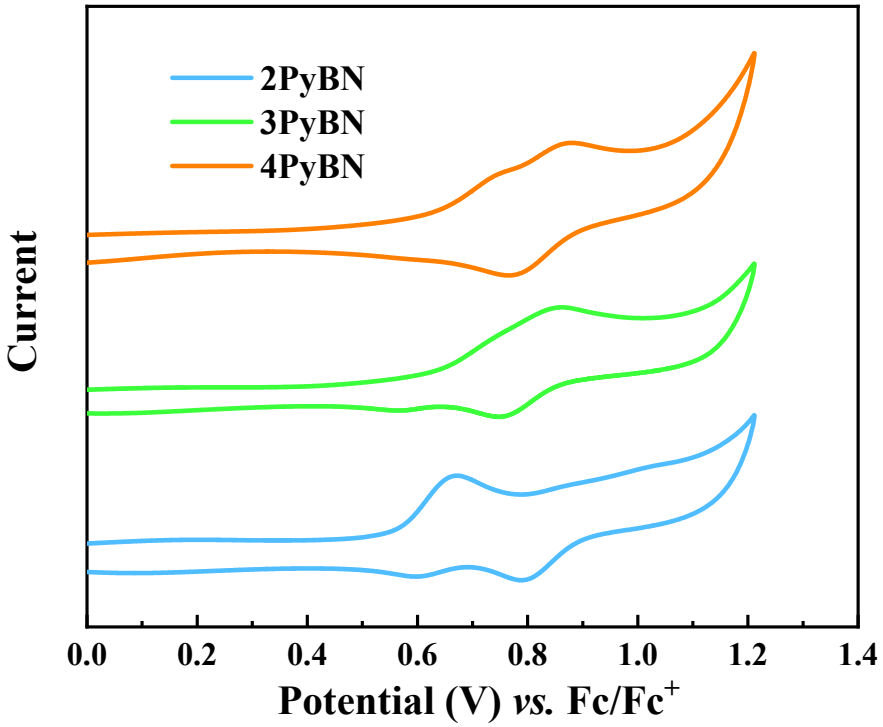

Fig. S10 CV curves of the emitters.

Table S1. Crystal data and structure refinement for 2PyBN and 4PyBN.

Molecule	2PyBN	4PyBN
Empirical formula	$C_{53}H_{56}BCl_4N_3$	$C_{53}H_{56}BCl_4N_3$
Formula weight	887.61	887.61
Temperature/K	120	170
Crystal system	triclinic	monoclinic
Space group	P-1	$P2_1/c$
a/Å	11.4044(4)	29.338(3)
b/Å	11.6590(4)	11.2565(11)
c/Å	18.3508(6)	16.2958(16)
α/°	77.6420(10)	90
β/°	77.5490(10)	90.366(3)
γ/°	83.5820(10)	90
Volume/Å^3	2321.88(14)	5381.4(9)
Z	2	4
ρ_{calc}g/cm^3	1.27	1.096
μ/mm^{-1}	0.295	0.254
F(000)	936	1872
Crystal size/mm^3	0.15 × 0.08 × 0.05	0.15 × 0.08 × 0.05
Radiation	MoKα (λ = 0.71073)	MoKα (λ = 0.71073)
2Θ range for data collection/°	3.932 to 52.834	3.748 to 52.834
Index ranges	$-14 \le h \le 14$, $-14 \le k \le 14$, $-22 \le l \le 19$	$-33 \le h \le 36$, $-12 \le k \le 14$, $-20 \le l \le 20$
Reflections collected	26851	37789
Independent reflections	9455 [R_{int} = 0.0625, R_{sigma} = 0.0776]	10722 [R_{int} = 0.0761, R_{sigma} = 0.0841]
Data/restraints/parameters	9455/3/562	10722/13/582
Goodness-of-fit on F^2	1.04	1.116
Final R indexes [I>=2σ (I)]	R_1 = 0.0969, wR_2 = 0.2507	R_1 = 0.1221, wR_2 = 0.3676
Final R indexes [all data]	R_1 = 0.1490, wR_2 = 0.3011	R_1 = 0.1741, wR_2 = 0.4253
Largest diff. peak/hole / e Å^{-3}	1.23/-0.86	0.57/-0.51

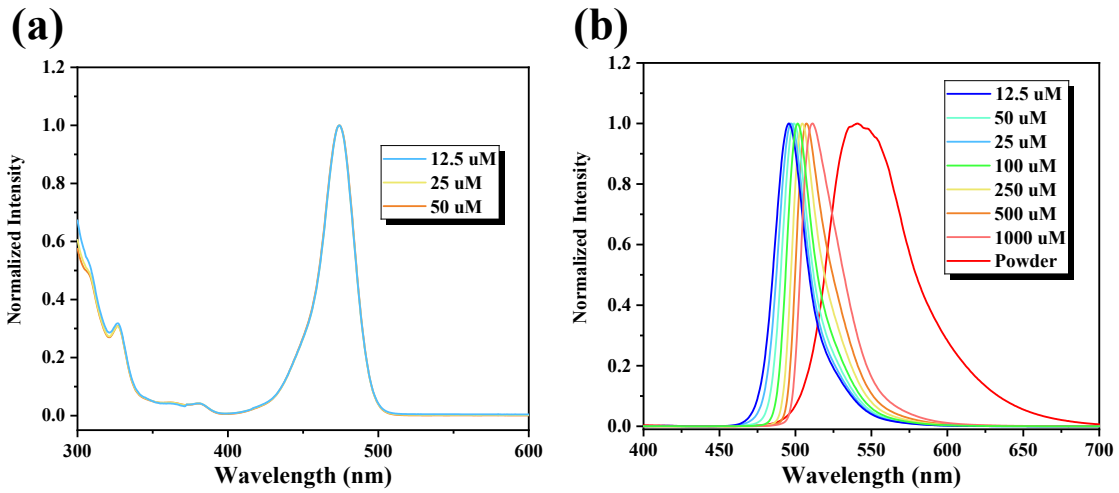

Fig. S11 Concentration dependent (a) UV-vis and (b) fluorescence spectra of 2PyBN in toluene solution at varies concentration and in crystal powder.

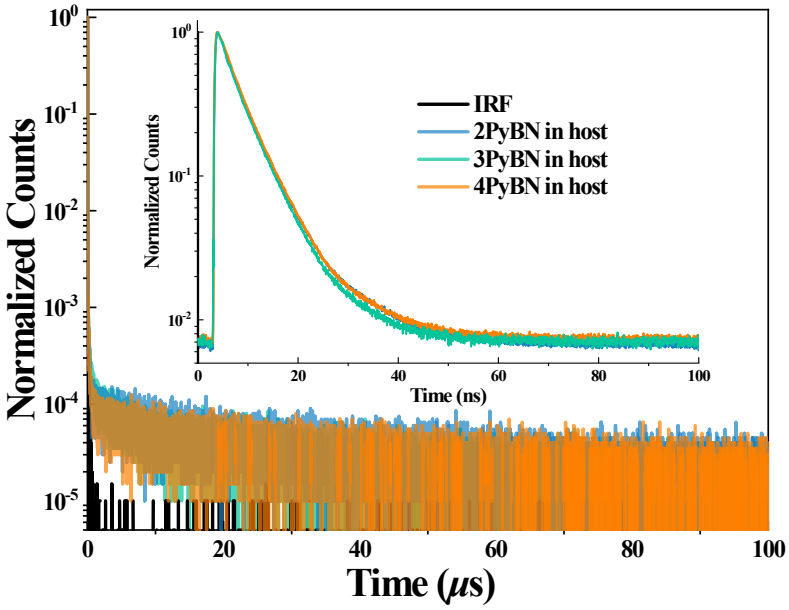

Fig. S12 Transient photoluminescence decay curves of 1% emitters in DMIC-TRZ host under inert atmosphere。

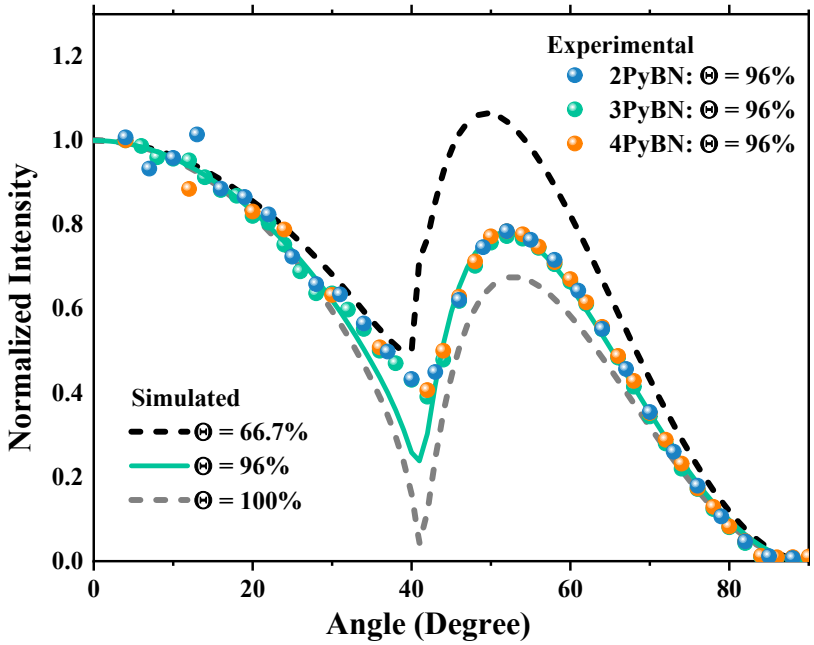

Fig. S13 Measured horizontal transition dipole moment ratios by angle-dependent p-polarized PL spectra of 1% emitters doped in DMIC-TRZ host.

Table S2. Kinetic parameters of the emitters in doped films.

Emitter	Φ_{PL} [a] (%)	Φ_p [b] (%)	Φ_d [b] (%)	τ_p [c] (ns)	τ_d [c] (μs)	k_r [d] (10^7 s^{-1})	k_{nr} [d] (10^7 s^{-1})	k_{ISC} [e] (10^7 s^{-1})	k_{RISC} [e] (10^4 s^{-1})
2PyBN	94	77	17	9.4	15.9	10.7	0.5	1.9	7.7
3PyBN	90	77	13	8.5	13.6	11.8	1.0	1.8	8.7
4PyBN	86	73	13	8.2	12.4	12.3	1.5	1.8	9.5

[a] Total photoluminescence quantum yield (Φ_{PL}); [b] Φ_{PL} contributions of the prompt component (p) and delayed (d) component; [c] lifetime of prompt and delayed fluorescence; [d] rate constant of radiative decay (k_r) and non-radiative decay (k_{nr}) from S_1 to S_0 states; [e] intersystem crossing (ISC) and reverse intersystem crossing (RISC) rate constants;

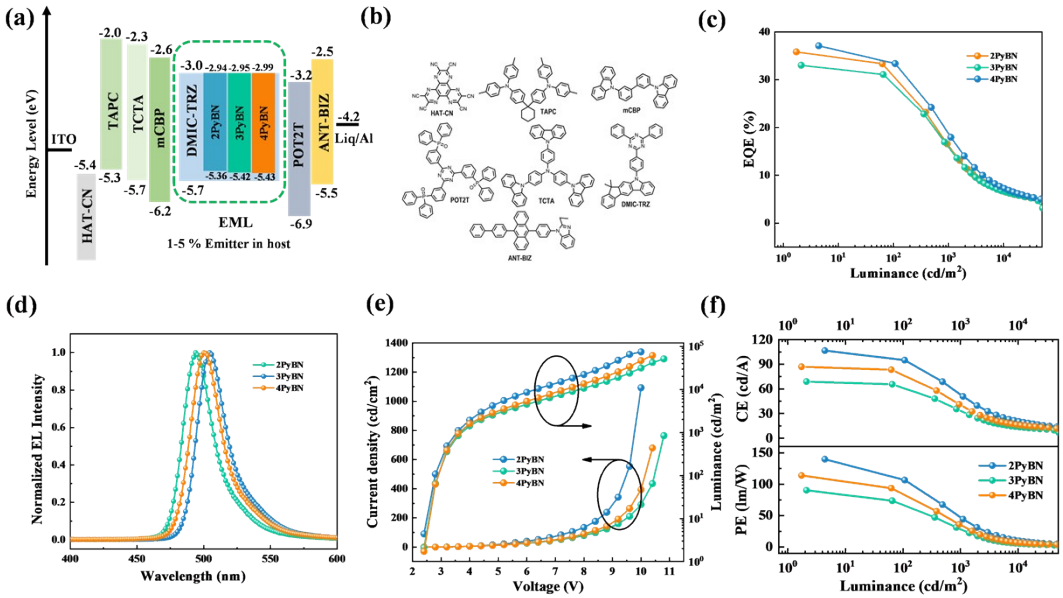

Fig. S14 (a) Device configuration and the energy level diagrams, (b) chemical structures of the materials, (c) EQE versus luminance curves, (d) the EL spectra, (e) luminescence and current density versus voltage characteristics, (f) CE/PE versus luminance curves the EL device using 1% emitter in the EL layer

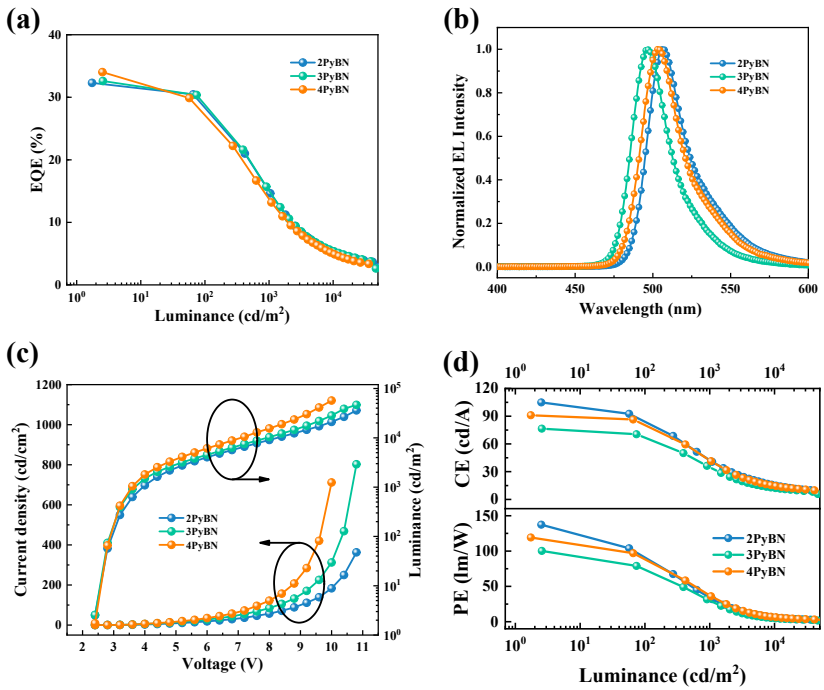

Fig. S15 (a) EQE versus luminance curves, (b) the EL spectra, (c) luminescence and current density versus voltage characteristics, (d) CE/PE versus luminance curves of

the EL device using 5% emitter in the EL layer

Table S3. Summary of the EL device data.

EML	V_{on} [a] (V)	L_{max} (cd/m^2)	λ_{EL} (nm)	FWHM (nm)	EQE [b] (%)	PE_{max} (lm/W)	CE_{max} (cd/A)	CIE (x, y)
2PyBN	2.4	36000	507	29	34.0/13.2/4.9	137.3	104.9	0.16, 0.67
3PyBN	2.4	46000	496	28	32.6/14.6/5.4	100.2	76.6	0.10, 0.53
4PyBN	2.4	57000	505	30	32.3/14.6/5.2	119.2	91.1	0.14, 0.63

[a] Turn-on voltage; [b] maximum, at 1000 and 10000 cd m^{-2}.

Table S4. The device performance of several representative green MR-OLEDs.

Emitter	λ_{EL} (nm)	FWHM	EQE (%)	Reference
2PyBN	505	26	38.0	This Work
3PyBN	494	28	37.8	This Work
4PyBN	501	29	36.8	This Work
2F-BN	501	40	22.0	1
3F-BN	499	38.5	22.7	1
4F-BN	493	31.6	20.9	1
m-Cz-BNCz	528	45	31.4	2
BBCz-G	515	54	31.8	3
AZA-BN	527	30	28.2	4
2PXZBN	522	60	17.7	5
2PTZBN	528	58	25.5	5
BN-DMAC	506	56	25.5	6
BN-DPAC	508	49	30.2	6
DtCzB-TPTRZ	520	41	30.6	7
TCz-B	515	30	29.2	8
BNSSe	515	50	35.7	9
BNSeSe	512	45	36.8	9
tCzphB-Ph	536	26	26.2	10
tCzphB-Fl	527	24	29.3	10
v-DABNA-CN-Me	504	23	31.9	11
BN-DP	528	36	35.1	12

BN-ICz	523	23	29.6	13
p[B-N] NO	525	31	27.6	14

Reference.

1. Y. Zhang, D. Zhang, J. Wei, Z. Liu, Y. Lu, L. Duan, *Angew. Chem. Int. Ed.* **2019**, *58*, 16912-16917.
2. Y. Xu, C. Li, Z. Li, Q. Wang, X. Cai, J. Wei, Y. Wang, *Angew. Chem. Int. Ed.* **2020**, *59*, 17442-17446.
3. M. Yang, I. S. Park, T. Yasuda, *J Am. Chem. Soc.* **2020**, *142*, 19468-19472.
4. Y. Zhang, D. Zhang, J. Wei, X. Hong, Y. Lu, D. Hu, G. Li, Z. Liu, Y. Chen, L. Duan, *Angew. Chem. Int. Ed.* **2020**, *59*, 17499-17503.
5. T. Hua, L. Zhan, N. Li, Z. Huang, X. Cao, Z. Xiao, S. Gong, C. Zhou, C. Zhong, C. Yang, *Chem. Eng. J.* **2021**, *426*, 131169.
6. P. Jiang, L. Zhan, X. Cao, X. Lv, S. Gong, Z. Chen, C. Zhou, Z. Huang, F. Ni, Y. Zou, C. Yang, *Adv. Opt. Mater.* **2021**, *9*, 2100825.
7. Y. Xu, C. Li, Z. Li, J. Wang, J. Xue, Q. Wang, X. Cai, Y. Wang, *CCS Chemistry* **2021**, 2077-2091.
8. M. Yang, S. Shikita, H. Min, I. S. Park, H. Shibata, N. Amanokura, T. Yasuda, *Angew. Chem. Int. Ed.* **2021**, *60*, 23142-23147.
9. Y. X. Hu, J. Miao, T. Hua, Z. Huang, Y. Qi, Y. Zou, Y. Qiu, H. Xia, H. Liu, X. Cao, C. Yang, *Nat. Photonics* **2022**, *16*, 803-810.
10. J. Liu, Y. Zhu, T. Tsuboi, C. Deng, W. Lou, D. Wang, T. Liu, Q. Zhang, *Nat. Commun.* **2022**, *13*, 4876.
11. S. Oda, T. Sugitani, H. Tanaka, K. Tabata, R. Kawasumi, T. Hatakeyama, *Adv. Mater.* **2022**, *34*, e2201778.
12. Y. Xu, Q. Wang, J. Wei, X. Peng, J. Xue, Z. Wang, S. J. Su, Y. Wang, *Angew. Chem. Int. Ed.* **2022**, *61*, e202204652.
13. X.-C. Fan, K. Wang, Y.-Z. Shi, Y.-C. Cheng, Y.-T. Lee, J. Yu, X.-K. Chen, C. Adachi, X.-H. Zhang, *Nature Photonics* **2023**.

14. G. Meng, H. Dai, J. Zhou, T. Huang, X. Zeng, Q. Wang, X. Wang, Y. Zhang, T. Fan, D. Yang, D. Ma, D. Zhang, L. Duan, *Chem Sci* **2023**, *14*, 979-986.